An active biopolymer network controlled by molecular motors

Gijsje H. Koenderink[a,b], Zvonimir Dogic[c,d], Fumihiko Nakamura[e], Poul M. Bendix[f], Frederick C. MacKintosh[g], John H. Hartwig[e], Thomas P. Stossel[e], and David A. Weitz[a,1]

[a]Department of Physics and Harvard School of Engineering and Applied Sciences, Harvard University, Cambridge, MA 02138; [b]FOM Institute for Atomic and Molecular Physics, Amsterdam 1098 SJ, The Netherlands; [c]Rowland Institute, Harvard University, Cambridge, MA 02142; [d]Physics Department, Brandeis University, Waltham, MA 02454; [e]Translational Medicine Division, Brigham and Women's Hospital, Department of Medicine, Harvard Medical School, Boston, MA 02115; [f]Niels Bohr Institute, 2100 Copenhagen, Denmark; and [g]Department of Physics and Astronomy, Vrije Universiteit, 1081 HV Amsterdam, The Netherlands

We describe an active polymer network in which processive molecular motors control network elasticity. This system consists of actin filaments cross-linked by filamin A (FLNa) and contracted by bipolar filaments of muscle myosin II. The myosin motors stiffen the network by more than two orders of magnitude by pulling on actin filaments anchored in the network by FLNa cross-links, thereby generating internal stress. The stiffening response closely mimics the effects of external stress applied by mechanical shear. Both internal and external stresses can drive the network into a highly nonlinear, stiffened regime. The active stress reaches values that are equivalent to an external stress of 14 Pa, consistent with a 1-pN force per myosin head. This active network mimics many mechanical properties of cells and suggests that adherent cells exert mechanical control by operating in a nonlinear regime where cell stiffness is sensitive to changes in motor activity. This design principle may be applicable to engineering novel biologically inspired, active materials that adjust their own stiffness by internal catalytic control.

active soft matter | cytoskeleton | filamin A | rheology | myosin II

Reconstituted biopolymer networks are a class of soft material that exhibits pronounced solidlike behavior while comprising only a few percent by volume of protein. They exhibit a rich mechanical behavior and pronounced nonlinearity (1). Moreover, they model important features of living cells, because the mechanics of cells are largely controlled by a network of filamentous proteins known as the cytoskeleton. Reconstituted networks comprising one of the principal components of the cytoskeleton, filamentous actin (F-actin), are interesting models for the rheology of semiflexible polymers. Like most filamentous protein networks, they are highly responsive to external stress. Cross-linked F-actin networks exhibit strong nonlinear stiffening with strain (1, 2). This phenomenon is particularly pronounced for the case of F-actin cross-linked by filamin A (FLNa), a widely represented protein that is essential for fetal development and cell locomotion (3). FLNa is a large, highly flexible dimer that promotes orthogonal F-actin cross-linking (4). FLNa–F-actin networks are very soft in their linear regime, with shear moduli as low as 1 Pa, yet they stiffen by up to three orders of magnitude in response to external shear stress (5–8). In this respect, FLNa–F-actin resembles the behavior of living cells, which also stiffen if subjected to (tensile) stress (9, 10). Cells, however, are not passive materials, but rather use molecular motors to convert chemical energy into mechanical work within the cytoskeleton. There is evidence that cells employ internal stress generated by myosin motors to modulate their mechanics (11–19). This suggests a strategy of creating a new class of active materials, whose elastic properties are controlled by enzymatic activity, through addition of myosin motors to a passive F-actin network.

In this article, we report that incorporating active and processive molecular myosin motors in FLNa–F-actin networks markedly increases network elasticity. The motors generate internal contractile stress in the network by pulling on F-actin filaments, which are linked to the network by the FLNa cross-links. This stress drives the network into a strongly nonlinear, stiffened regime. These results suggest that actomyosin contractility allows adherent cells to operate in a nonlinear regime to control their mechanics actively. The experimental system represents a recently discovered class of active soft materials—gels whose elasticity can be precisely tuned over three orders of magnitude by enzymatic activity. Moreover, unlike passive glassy materials, which are inherently pinned in a nonequilibrium state, these materials are driven into nonequilibrium through the internal conversion of chemical energy to mechanical energy.

Results

Experimental Design. We used a network of actin filaments cross-linked with FLNa and with embedded myosin II motors that actively apply contractile forces. Myosin II is a two-headed motor protein that moves toward the plus end of an actin filament (Fig. 1A Upper). Individual myosin motors are nonprocessive at physiological (mM) ATP concentrations, spending only 2% of their chemomechanical cycle attached to F-actin (20). To enable sustained generation of tension, myosin was assembled into thick filaments with an average length of about 1 μm according to electron microscopy (Fig. 1B), or about 300 myosin molecules per filament (21). We thus mimicked the mechanism used by nonmuscle cells, where myosin II is assembled into similar, although smaller, filaments (22). Such myosin filaments are bipolar, with the motor tails in the center and the motor heads on both ends (Fig. 1A Lower). The filaments are effectively processive, because at any given time, one or more motor heads are bound to an actin filament. In the absence of elastic constraints, myosin filaments fluidize actin networks by actively sliding antiparallel actin filaments past one another (23–25). To accommodate internal stress buildup, we prevented sliding by cross-linking the actin filaments with recombinant human FLNa.

Rheology of Actin Networks. We measured the mechanical properties of the reconstituted F-actin networks polymerized in a cone and plate rheometer. We applied a small oscillatory stress, $\sigma(\omega)$, at a frequency ω, and monitored the resultant strain, $\gamma(\omega)$. Solutions of actin filaments were rather weak. The elastic modulus, $G'(\omega)$, was of order 0.8 Pa and depended weakly on frequency (solid black line in Fig. 1C Upper). Over the frequency range studied, the elastic modulus dominated over the viscous modulus, $G''(\omega)$, although the loss tangent, $\tan \delta = G''(\omega)/G'(\omega)$, was close to 1 (solid black line in Fig. 1C Lower). Cross-linking with FLNa made the network only

Fig. 1. Effect of myosin II motors on the linear rheology of F-actin solutions and networks. (*A*) Myosin II motors (blue) are two-headed, bind to an actin filament (gray), and move toward its plus end (*Upper*). They multimerize to form processive, bipolar filaments that slide two antiparallel actin filaments toward one another (*Lower*). (*B*) Electron micrograph of reconstituted myosin II thick filaments. (*C*) Frequency dependence of the elastic shear modulus (*Upper*) and loss tangent (*Lower*) of F-actin solutions (solid black line, passive; white squares, active), and cross-linked F-actin networks (gray open triangles, passive; blue solid squares, active; magenta solid squares, myosin activity blocked by blebbistatin). The loss tangent is fairly noisy because it is the ratio of G'' to G', where G'' is typically five times smaller than G'. Molar ratios are [myosin]/[actin] = 0.02 and [FLNa]/[actin] = 0.005, all at 5 mM ATP. (*D*) Dependence of stiffness on concentration of myosin (*Left*) for [FLNa]/[actin] ratios of 0 (gray open triangles), 0.005 (blue squares), and 0.010 (solid red triangles); and FLNa (*Right*) for [myosin]/[actin] ratios of 0 (gray open triangles), 0.02 (blue squares), and 0.05 (solid red triangles). The bottom *x* axis expresses concentrations in molar ratio relative to actin, and the top *x* axis uses numbers of FLNa dimers or myosin filaments per actin filament. Lines are power law fits with exponents 0.17 and 0.79 (*Right*).
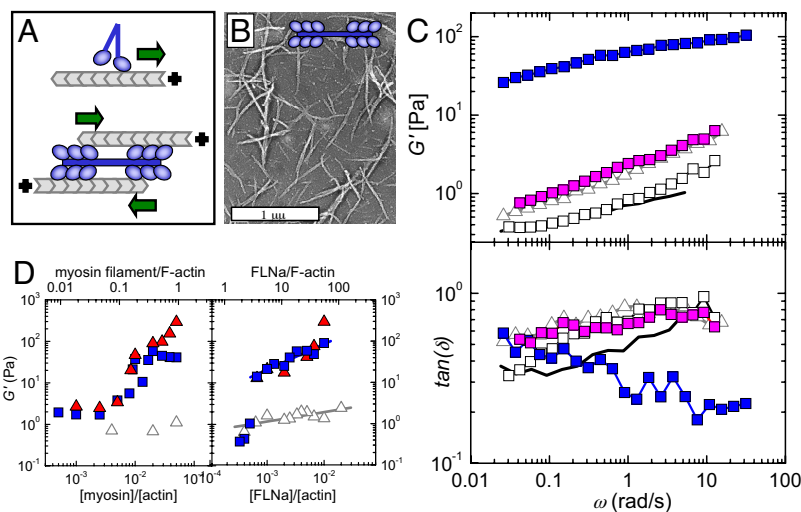
slightly stiffer (gray open triangles in Fig. 1*C Upper*). Based on previous modeling and experimental results, we interpret this finding as resulting from the cross-linking of rodlike F-actin by relatively flexible cross-links (8, 26). In this situation, the stretching of the flexible cross-linkers dominates the linear modulus. FLNa molecules have a contour length of 160 nm and persistence length of 20 nm, and they are therefore large and floppy compared with F-actin (27). The loss tangent was somewhat enhanced in the presence of FLNa, reflecting enhanced dissipation (open triangles in Fig. 1*C Lower*). However, addition of myosin II thick filaments to the cross-linked network imparted an enormous increase in stiffness, by almost two orders of magnitude (blue solid squares in Fig. 1*C Upper*). At the same time, myosin addition substantially lowered the loss tangent, indicating a more solidlike response (blue squares in Fig. 1*C Lower*).

We observed a marked threshold effect of motor concentration on network elasticity. The motors had a negligible effect on network stiffness at low myosin concentration, but they strongly stiffened the network above a molar ratio of [myosin]/[actin] ≈ 0.01 (Fig. 1*D Left*). The threshold value was independent of FLNa concentration, at least at [FLNa]/[actin] ratios above 0.0007. We observed a similar threshold effect of FLNa concentration. Myosin had no appreciable effect on network stiffness at low FLNa concentrations, but it exerted appreciable stiffening above [FLNa]/[actin] ≈ 0.0007 (Fig. 1*D Right*). This observation held for any myosin concentration sufficiently high to exert significant stress. FLNa and myosin were required together to attain active stiffening, as demonstrated by the low values of G' in the absence of either component (gray open triangles in Fig. 1*D*). These threshold levels are best interpreted in terms of actin filaments and myosin thick filaments, instead of actin and myosin monomers. Given an average length for the actin filaments of 15 μm (or 5,100 monomers), the threshold concentrations for stiffening were one myosin filament for every five actin filaments, and three FLNa cross-linkers for every actin filament (top *x* axis in Fig. 1*D*). We found that varying FLNa and myosin concentrations at fixed actin filament length had the same effect on network stiffness as varying the average actin filament length (with the capping protein gelsolin) for fixed FLNa and myosin concentrations (Fig. S1). This confirms that the number of myosin thick filaments and FLNa cross-linkers per actin filament are useful control parameters. Remarkably, for a fixed concentration of actin (23.8 μM), we can tune $G'(\omega)$ over two orders of magnitude, from only 0.3 Pa to values as high as 300 Pa. The number of binding sites on actin filaments for myosin and FLNa presumably limits maximum stiffness.

We also expect a strong dependence of the elastic modulus on

actin concentration, because stiffening arises from the simultaneous interaction of a myosin thick filament with two actin filaments, as sketched in Fig. 1*A*. To test this prediction, we measured the variation of $G'(\omega)$ with actin concentration for networks with fixed molar ratios of [FLNa]/[actin] = 0.01 and [myosin]/[actin] = 0.02. We indeed observed a very strong increase of $G'(\omega)$ with increasing actin concentration for both long (15 μm) and short (1.5 μm) filaments (Fig. S2). The increase occurred at lower actin concentrations for the longer filaments, because they entangled at a lower concentration.

Effect of Myosin Motor Activity on Network Rheology. The presence of myosin motors can itself lead to cross-linking (24). However, we used a high ATP concentration, where individual myosin heads remained bound only for about 1 ms (20), which is unlikely to lead to cross-linking. To validate this prediction, we removed all cross-linking proteins by making an F-actin solution in the absence of FLNa. In this case, we found no effect of myosin on the elastic modulus of the actin solution (white squares in Fig. 1*C*). Thus, in the presence of these high ATP levels, myosin itself does not crosslink F-actin. Instead, it must be the motor activity of the myosin that leads to stiffening. As further confirmation, we added blebbistatin, a drug that inhibits myosin's ATPase activity without inducing permanent binding (28). We found that 1 mM blebbistatin completely eliminated stiffening: the elastic modulus (magenta squares in Fig. 1*C Upper*) was then indistinguishable from that of passive actin–FLNa networks in the absence of motors (gray open triangles in Fig. 1*C Upper*). Thus, the myosin filaments stiffened the actin networks by an active mechanism, but only in the presence of FLNa. This is consistent with previous reports that myosin activity leads to stiffening in the presence of cross-links (29) but not in their absence (24). The loss tangent of the active actin solution (white squares in Fig. 1*C Lower*) was slightly increased compared with that of a passive solution (solid black line in Fig. 1*C Lower*), indicating that the motors led to increased viscous dissipation.

Effects of Myosin on Network Architecture. Stiffening likely arises from relative sliding of actin filaments by the myosin filaments. Because the actin filaments are cross-linked into the network, this induces a local tension, as sketched in Fig. 2*D*. However, this perturbation may also cause some reorganization of the network. In bundled F-actin networks, myosin filaments have been observed to cause network contraction (30) and pattern formation (31). To investigate possible reorganization of the structure of actin–FLNa networks by myosin in the presence of mM levels of ATP, we labeled the actin filaments fluorescently by Alexa488-phalloidin
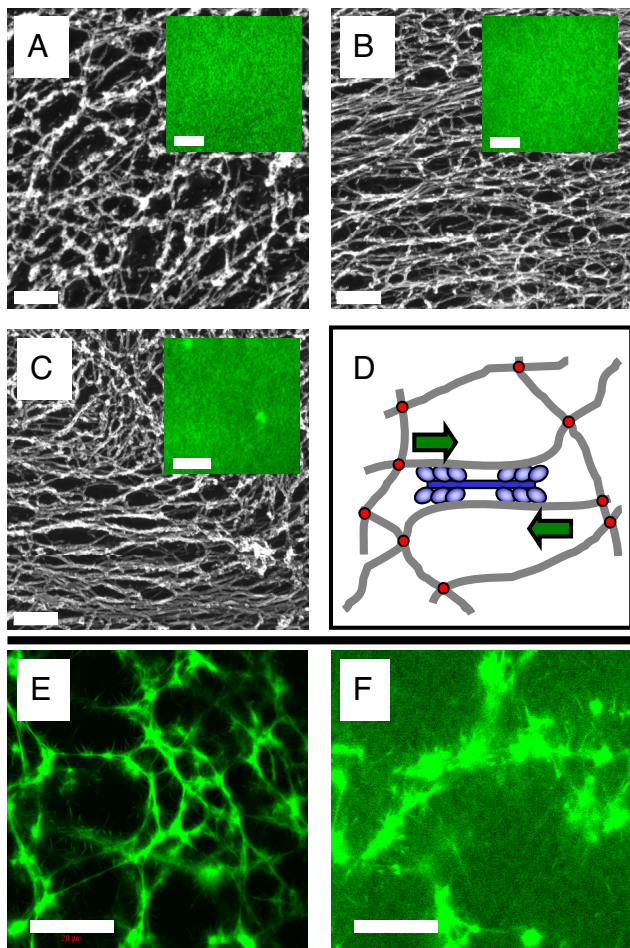
Fig. 2. Microstructure of passive and active F-actin solutions and networks visualized by electron microscopy (*A–C*) and fluorescence microscopy (*A–C Insets, E*, and *F*). (*A*) Passive solutions are isotropic, homogeneous, and unbundled. (*B*) Active solutions ([myosin]/[actin] = 0.02 and 5 mM ATP) are still homogeneous (*Inset*), but the myosin locally aligns and bundles the actin filaments. (*C*) Active networks ([FLNa]/[actin] = 0.005, [myosin]/[actin] = 0.02, 5 mM ATP) are macroscopically homogeneous, but small contractile foci are present (*Inset*); the actin filaments extending out from these foci are bundled and aligned, but they merge into a more isotropic network between the foci. (*D*) Proposed mechanism of active stiffening: myosin filaments (blue) contract actin filaments (gray) toward one another, thereby pulling against the FLNa cross-links (red) and generating an internal stress. (*E* and *F*) Passive networks cross-linked by rigor myosin (0 mM ATP) show bundles and clumps, both in the presence (*E*) and absence (*F*) of FLNa. For all panels, [actin] = 23.8 μM, and the average filament length is 15 μm. F actin is fluorescently labeled by Alexa488-phalloidin. (Scale bars: Insets *A–C* and *F*, 10 μm; *A–C*, 200 nm; *E*, 20 μm).
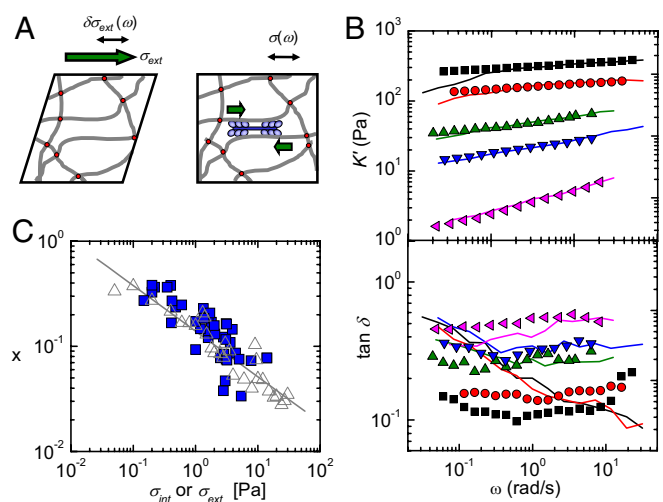

Fig. 3. Comparison of the effects of internal, myosin-driven stress and external shear stress on the rheology of F-actin networks. (*A*) Passive networks are subjected to a constant external shear stress, and their differential moduli are measured by superposing a small oscillatory stress (*Left*). Active networks are internally stressed by motors, and their linear moduli are measured by applying a small oscillatory stress; because of the internal prestress, this is equivalent to a differential measurement (*Right*). (*B*) Frequency dependence of the elastic modulus (*Upper*) and loss tangent (*Lower*). Lines correspond to active networks (bottom to top: [myosin]/[actin] = 0.005, 0.009, 0.010, 0.039, and 0.050), whereas symbols correspond to passive networks (bottom to top: σ_{ext} = 0.35, 1.6, 3.1, 7.8, and 12 Pa). The [FLNa]/[actin] ratio is 0.01. (*C*) The power law exponent, *x*, characterizing the frequency dependence of *G'*, decreases with stress in the same manner for passive networks (stressed by σ_{ext}) and active networks (stressed by σ_{int}). The line is a power law fit with slope 0.43.

and imaged the networks by fluorescence microscopy. At an actin concentration of 23.8 μM (1.0 mg/mL), solutions of F actin were isotropic, homogeneous, and unbundled (Fig. 2*A Inset*). Upon addition of myosin, there was no noticeable change in network structure (Fig. 2*B Inset*). When myosin and FLNa were both present, the network still remained homogeneous and unbundled (Fig. 2*C Inset*). However, we observed small regions of compacted actin dispersed in a homogeneous, isotropic matrix of entangled actin filaments. The fact that these contractile foci were formed only in the presence of FLNa confirms a cross-linking requirement for local network contractility. High-resolution images obtained by electron microscopy confirm the fluorescence microscopy observations that F-actin solutions are homogeneous and unbundled (Fig. 2*A*), and that they remain so upon myosin addition (Fig. 2*B*). However, electron microscopy reveals that myosin creates regions

where actin filaments are somewhat more aligned. We also observed occasional contractile foci ([Fig. S3](#)), which may correspond to the foci seen with confocal microscopy. The alignment of filaments, observed both in the absence of FLNa (Fig. 2*B*) and in its presence (Fig. 2*C*), is likely due to longitudinal binding of the myosin filaments along actin filaments. However, there is no evidence of alignment in the larger field of view observed in the light microscopy, suggesting that this binding has a limited role, if any, in the elasticity of the network. This interpretation is consistent with the rheology data, which show that myosin stiffens actin–FLNa networks by enzymatic activity, not by cross-linking. By contrast, in actin–myosin networks formed under rigor (0 mM ATP) conditions, where myosin permanently binds to F-actin, the myosin filaments dramatically changed the network structure. Both with (Fig. 2*E*) and without (Fig. 2*F*) FLNa, large F-actin aggregates and bundles were visible, in contrast to the network structure with active myosin motors.

Calibration of Myosin-Generated Stress. Application of an external shear stress to actin–FLNa networks also leads to stiffening (5, 6, 8). This effect provides a means to calibrate the degree of internal stress produced by motors in active networks. We therefore compared the rheology of active networks stiffened by myosin with that of passive networks under shear, as sketched in Fig. 3*A*. We applied a time-independent, external stress, σ_{ext}, to the passive networks and measured the differential elastic, *K'*, and viscous, *K''*, moduli from the strain response to a small, superimposed oscillatory stress, $\delta\sigma_{ext}(\omega)$ (2, 5, 6, 8, 9). We note that the cross-linked networks display no creep (8), ensuring that this differential technique is the optimal method for measuring the nonlinear response, unlike in the case of entangled F-actin solutions, which exhibit appreciable creep (32).

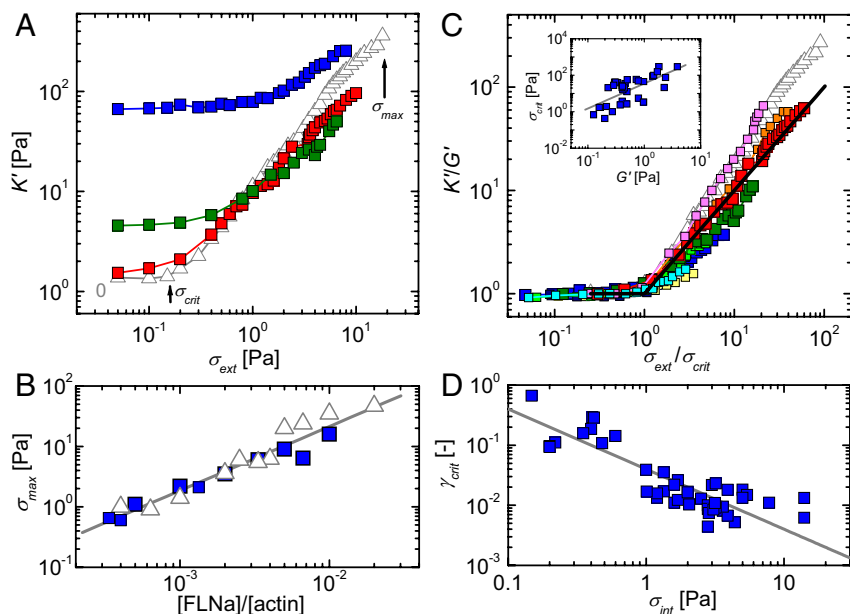Upon application of an increasingly large, steady shear stress, the

Fig. 4. Nonlinear response of passive and active F-actin networks to an external shear stress. (A) Stress-stiffening curves for active networks [with myosin to actin ratios of 0.02 (blue), 0.005 (green), and 0.001 (red)] and a passive network (gray open triangles) at a fixed [FLNa]/[actin] ratio of 0.005. Arrows indicate critical stress (σ_{crit}) and rupture stress (σ_{max}) for the passive network. (B) The rupture stress increases linearly with FLNa concentration, independently of the myosin content. (C) Normalized stress-stiffening curves collapse onto a single master curve with a power law stiffening regime, $K' = G'\sigma^1$ (black line). The [FLNa]/[actin] ratio is 0.005. The [myosin]/[actin] ratios are 0 (gray), 0.0005 (magenta), 0.001 (red), 0.0025 (orange), 0.005 (olive), 0.008 (green), 0.0133 (navy), 0.0167 (yellow), 0.02 (blue), and 0.0286 (turquoise). (Inset) Relation between the scaling factors, according to $G' \propto \sigma_{crit}^{1.3}$ (gray line). (D) The critical strain decreases as the level of motor-driven stress increases, according to an approximate power law, $\gamma_{crit} \propto \sigma^{-1}$ (solid line).

passively deformed F-actin–FLNa networks increasingly stiffened (symbols in Fig. 3B Upper) and became more solidlike. The differential stiffness became more weakly dependent on frequency, and the loss tangent, $\tan \delta = K'/K''$, decreased (Fig. 3B Lower). Similarly, when the networks were made active by embedding myosin thick filaments, the stiffness increased with increasing motor concentration (lines in Fig. 3B Upper). Strikingly, for every concentration of myosin thick filaments, we were able to apply an external shear stress that yielded an identical elastic modulus for all frequencies, as shown by the comparison of the lines (active networks) and symbols (passively deformed networks). The viscous responses reveal subtly different microscopic dynamics. At the highest values of stress, a noticeable discrepancy appeared at frequencies below 0.2 rad/s: the active networks exhibited a small decrease in the elastic modulus with a concomitant increase of the loss tangent, indicative of increased dissipation (Fig. 3B Lower). In contrast, the loss tangent for passive networks under high levels of external stress was nearly frequency-independent. This discrepancy suggests that in the active networks, stress relaxation occurs on time scales longer than about 5 s, possibly resulting from myosin motor release. This time scale is consistent with the typical release rate of myosin filaments observed in microrheology of F-actin–myosin solutions (33).

An external shear stress is anisotropic, and therefore is borne primarily by a small number of highly oriented filaments (2, 34). By contrast, internal myosin-generated stress is expected to be isotropic, and therefore can affect a much larger number of filaments (29, 35, 36). Nevertheless, the close correspondence of the elasticity of active and passive networks under stress enabled us to calibrate the effective internal stress, σ_{int}, applied by the myosin motors. The maximum level of internal stress achieved corresponded to an externally applied shear stress of $\sigma_{ext} = 14$ Pa (Fig. S4). We approximated the maximum force per myosin filament, F, by assuming an isotropic internal stress and by using an average area per filament, $\xi^2 \approx 0.1\ \mu m^2$, where ξ is the network mesh size. We obtained $F \approx 1$ pN, consistent with only a few myosin heads active at any given time in each myosin filament, each having a stall force of 4 pN (20). This finding agrees with complementary findings that we reported recently on actin–myosin networks (30, 33).

The increased stiffness of the network upon activation of internal stress can also be characterized by the exponent, x, of the power law dependence of stiffness on frequency, $K'(\omega) \propto \omega^x$. For a purely

elastic solid, x is zero; for a purely viscous liquid, x is one. The actin–FLNa networks are viscoelastic and have an intermediate exponent of about 0.4 in the unstressed state. Upon application of external shear stress to a passive network, the exponent decreased to a value close to zero as the level of stress was raised (Fig. 3C, gray open triangles). Upon incorporation of motors and ATP, the exponent decreased in the same manner as the motor concentration was raised (Fig. 3C, solid blue squares). This consistency again emphasizes the close analogy of motor-driven stress to the effect of an external shear stress.

Nonlinear Response. The effect of the motors is to induce internal tension that brings the network into a nonlinear state. Upon application of an additional steady shear stress, the network exhibits an apparently linear response over an extended range of applied stress. However, with sufficiently large applied stress, larger than a critical stress (σ_{crit}), the network again begins to stiffen. This is illustrated for an active network with [myosin]/[actin] = 0.02, whose stiffness was 100 Pa in the linear regime, nearly two orders of magnitude above that of an unstressed network (blue solid squares in Fig. 4A). Upon lowering the [myosin]/[actin] ratio to 0.005 (green solid squares), or further to 0.001 (red solid squares), both the initial elastic modulus and σ_{crit} decreased (see Fig. 4A). By contrast, the passive network had a linear modulus of only 1 Pa but started to stiffen at a much smaller σ_{crit} (gray open triangles). Strikingly, at large shear stress values, the nonlinear response of the active networks asymptotically approached the same stiffness as that of the passive network. Moreover, passive and active networks all broke at approximately the same maximum shear stress, σ_{max} (indicated by an arrow in Fig. 4A). This rupture stress increased linearly with FLNa concentration (Fig. 4B), suggesting that forced unbinding of FLNa is the dominant failure mode (8, 26). This type of behavior is typical of weakly binding cross-linkers (37) and contrasts with strongly cross-linked networks, where the dominant failure mode is actin filament rupture (2, 34). If we assume that all cross-linkers equally share the load, we estimate a typical failure force per FLNa cross-link of about 2 pN. The correspondence of the stiffening response of active and passive networks at large shear stresses suggests that the effect of preexisting internal stress generated by motors is equivalent to the effect of an external shear stress. Consistent with this interpretation, the stiffening curves in Fig. 4A can be collapsed onto a single master curve by normalizing

PHYSICS

K' by its zero-stress value, G', and σ_{ext} by σ_{crit}, as shown in Fig. 4C. Stress-stiffening in the nonlinear regime is well approximated by a power law with a slope of 1, shown by the solid black line in Fig. 4C.

Although the critical stress increased upon addition of active motors, the corresponding critical strain, γ_{crit}, decreased, as shown in Fig. 4D. Passive actin–FLNa networks stiffen strongly above $\gamma_{\text{crit}} \approx 30\%$. This value of critical strain reflects the difference in compliance between the FLNa cross-linkers and the actin filaments (8, 26). At small strain, the network compliance is dominated by the soft FLNa cross-linkers. Upon application of a shear stress, the thermal fluctuations of the cross-linkers are pulled out. When the cross-linkers reach their full extension, the network suddenly becomes incompliant because the actin filaments have a much larger persistence length of 15 μm. The network therefore stiffens when the strain exceeds a critical value that is proportional to the contour length of the cross-linker (26). Upon addition of motors, the critical strain decreases substantially to a final value of only 0.6% at the highest [myosin]/[actin] ratio of 0.02. Data for different FLNa and myosin concentrations may be combined by plotting the critical strain as a function of internal tension, which shows that $\gamma_{\text{crit}} \propto \sigma_{\text{int}}^{-1}$ (line in Fig. 4D). This is a manifestation of the preexisting tension in the network generated by the motors: the myosin motors actively pull against the FLNa cross-links, thereby pulling out thermal fluctuations of the FLNa cross-linkers and the actin filaments. A very small, externally applied shear strain is then sufficient to bring the actively prestressed network out of its linear regime.

Discussion

Our data identify two key design principles of active biopolymer networks whose mechanical properties are controlled by the addition of molecular motors. The first principle is that the motors must be sufficiently processive. Nonprocessive myosin subfragments indeed do not cause active stiffening (38). The second principle is that F-actin cross-linkers must be present to provide sites for mechanical anchorage, thus accommodating buildup of internal tension (30, 31, 39). In the absence of cross-linkers, myosin filaments weaken F-actin solutions by active filament sliding (23–25). Moreover, cross-linking serves to make the actin network sensitive to an applied tension.

In vitro studies have shown that strain-stiffening is a generic feature of cross-linked F-actin networks. However, the quantitative form of the nonlinear response depends on the nature of the cross-linking protein. For small, rigid cross-links, strain-stiffening results from the nonlinear entropic stretching modulus of the actin filaments (1, 2, 34, 40). The large, compliant cross-linker FLNa significantly enhances the strain-stiffening response (5, 6, 8): FLNa–F-actin networks are soft at small strain but stiffen strongly and have a large rupture stress (26). We found that addition of motors to an FLNa cross-linked network directly mimics the effect of an external shear stress, dramatically stiffening the network. By contrast, we found that scruin, an incompliant cross-linker, does not promote active stiffening of F-actin networks upon addition of myosin (cf. Fig. S5). We ascribe this to the weaker stress-stiffening response evoked by this cross-linker. Intriguingly, stiffening of actin networks cross-linked by rigid biotin–streptavidin linkages is only reported at ATP concentrations in the micromolar range (29). At such low ATP concentrations, myosin is 1,000-fold more processive (20), and the system is also close to rigor. To resolve the intriguing difference between the response of flexibly and rigidly cross-linked networks to motor activity, it will be interesting to systematically change the degree of motor processivity by adjusting ATP and salt levels.

Our model system provides a platform to analyze the role of active motors in the rheology of actin networks in a quantitative manner. Because the motors pull on actin filaments that are cross-linked by FLNa, there is likely cross-talk between the activity of myosin and FLNa. Myosin-driven tension may, for instance, release FLNa cross-linking. Evidence exists for tension-dependent cross-linker binding kinetics both in vitro (41) and in vivo (19, 42).

Recently, FLNa was shown to unbind at forces in a range of 5–100 pN (43). The viscous response of our reconstituted networks shows signatures of FLNa and/or myosin unbinding. It will be interesting to measure on/off rates of both proteins directly (4). Our data suggest that the mechanical and kinetic properties of the cross-linkers should be included in theoretical models of active polymer networks (23, 35, 36, 44–46).

Our work also may provide mechanistic insights into cellular mechanics. It supports the observation that myosin-generated prestress contributes to cell stiffness (9, 12–14, 18, 47) and provides a physical explanation for this phenomenon, which was hitherto lacking. The rheology of our reconstituted system exhibits remarkable similarity to the mechanical properties reported for cells. The active stiffening effect increases with motor concentration and vanishes when motor activity is inhibited by blebbistatin. Similar effects are observed in adherent cells during interphase (11–18) and mitosis (19, 47). The active stiffening effect also increases when the cross-linker concentration is increased. This is reminiscent of recent observations in adherent *Dictyostelium* amoeboid cells, where cross-linkers were shown to enhance cortical tension as well as cell stiffness (19). The elastic modulus increases with frequency, according to a weak power law with an exponent that decreases when motors actively tense the network. This was also observed for smooth muscle cells (14, 48). Myosin generates the same stiffening of F-actin–FLNa networks as an external shear stress. This is in striking agreement with experiments on single fibroblasts, where active cell contraction and external cell stretching also yielded identical stiffening (9). The stress-stiffening curves of our active, reconstituted networks can be rescaled onto a single master curve, when the tangent stiffness is normalized by its zero-force value and the external stress by the critical stress. This master curve matches the master curve that was found for fibroblasts, with a linear dependence of scaled modulus on scaled stress in the nonlinear regime. Both for the cells and for our reconstituted system, the myosin-dependent scaling factors are related by a power law, $G' \propto \sigma_{\text{crit}}^{y}$, with exponent $y \approx 1.3$ (Fig. 4C Inset), not far from an exponent of 1 expected based on the stress-stiffening exponent. Our data suggest that adherent cells inherently operate in a nonlinear, stress-stiffened regime driven by actin–myosin contractility. The precise control over network stiffness afforded by variation of myosin and FLNa concentrations suggests that cells may spatially and temporally control their stiffness at multiple levels.

Despite the qualitative resemblance to the myosin-dependent rheology of cells, the reconstituted networks still have elastic moduli about an order of magnitude lower than those typically reported for adherent cells (0.5–10 kPa; refs. 12, 13, and 49–51). Although we used molar ratios of FLNa and myosin relative to actin that are similar to those in cells (22, 52, 53), the filament length in most of our experiments was longer (15 μm compared with $\approx$1–2 μm in cells; ref. 53) and the absolute concentration of actin lower (1 mg/mL, compared with $\approx$10 mg/mL in cells; ref. 53). Indeed, in the reconstituted system, motor-driven stiffening is strongly dependent on filament length and actin concentration. Moreover, in cells, FLNa acts in concert with numerous other cross-linking proteins. An interesting question is whether FLNa has a specific role in the myosin-dependent rheology of cells (52). Another key question is: what is the locus of tension generation in nonmuscle cells? Myosin II is present in the cell cortex but also in stress fibers (22). Our work suggests that it may not be necessary for actin–myosin to be assembled into highly ordered stress fibers to generate stiffening.

The active protein networks studied here belong to a new class of active soft materials inspired by the cellular cytoskeleton. Such materials evoke fundamental questions: they are driven far out of equilibrium, so equilibrium concepts, such as causality in oscillatory shear rheology, may break down. Even concepts that can be applied to other nonequilibrium systems, such as glasses, may not hold. Even though glasses are out of equilibrium, over certain time scales they behave as if they are in quasiequilibrium. It is an open question

whether an active material driven by motors behaves in a similar way. Finally, integration of molecular motors into (bio)polymer networks is an interesting design principle for new, self-assembling "smart" materials that actively adapt to external stimulation (54).

Materials and Methods

Protein Preparation. Monomeric (G) actin was purified from rabbit skeletal muscle (55), with a gel-filtration step (HiLoad 16/60 Superdex 200 pg, GE Healthcare). Actin was stored in G buffer (2 mM Tris·HCl, 0.2 mM ATP, 0.2 mM CaCl$_2$, 0.2 mM DTT, and 0.005% NaN$_3$, pH 8.0). Myosin II was obtained from chicken skeletal muscle and stored in a high-salt buffer [0.6 M KCl, 1 mM DTT, 50 mM phosphate (pH 6.3), and 50% glycerol]. Fresh myosin solutions were prepared by dialysis against AB300 buffer (300 mM KCl, 4 mM MgCl$_2$, 1 mM DTT, and 25 mM imidazole, pH 7.4). Recombinant human plasma gelsolin and human FLNa were purified from *Escherichia coli* (56) and Sf9 cell lysates (4).

Sample Preparation. Reconstituted networks were prepared in assembly buffer (25 mM imidazole, 50 mM KCl, 5 mM MgATP, 0.2 mM CaCl$_2$, and 1 mM DTT, pH 7.4). The ATP concentration was sufficiently high to prevent ATP depletion during a period of at least 4 h after sample mixing, as evidenced by microscopy and rheology. The actin concentration was 23.8 μM (1.0 mg/mL) unless specified otherwise. The average filament length in the absence of gelsolin was 15 μm. To create filaments of defined lengths, actin was polymerized in the presence of increasing concentrations of gelsolin (the average length is determined by the molar ratio of gelsolin to actin).

Rheology. Reconstituted networks were polymerized at 25 °C in the cone and plate geometry (20 mm, 1°) of a stress-controlled Bohlin C-VOR rheometer (Malvern Instruments). The linear storage and loss moduli, G' and G'', respectively, were measured by applying a small sinusoidal stress and measuring the resultant strain. The elastic modulus in the nonlinear regime was measured by superposing a small oscillatory stress of magnitude ($\partial\sigma_{ext}$) onto a constant prestress (σ_{ext}). Because the F-actin-FLNa networks show very little creep, we can compute the differential modulus, $K^*(\omega,\sigma_{ext}) = [\delta\sigma(\omega)/\delta\gamma(\omega)]|\sigma_{ext}$, from the resultant oscillatory strain, $\delta\gamma$. We used oscillatory stress amplitudes $\delta\sigma_{ext}/\sigma_{ext} < 0.1$, limiting $\delta\gamma$ to ≈1%. The elastic and viscous components are referred to as K' and K''. Where an elastic modulus is reported at a single frequency, $\omega = 0.63$ rad/s.

Electron Microscopy. Actin solutions were polymerized on a poly-L-lysine-coated coverslip in 2 mM MgCl$_2$ and 10 mM KCl; the myosin filaments were unchanged by these conditions. After incubation for 45 min at room temperature, the samples were rapidly frozen without fixation. Frozen samples were transferred to a liquid nitrogen-cooled stage on a Cressington CFE-60 apparatus, warmed to −120 °C, and the tops were carefully scraped with a liquid nitrogen-cooled knife. Samples were dried at −95 °C for 20 min and metal-cast with 1.4 nm of platinum (45° with rotation) and 5 nm of carbon (90° without rotation). Metal replicas were floated from the coverslips in 25% hydrofluoric acid, water-washed, and examined by transmission electron microscopy (JEOL 1200-EX).

1. Storm C, Pastore JJ, MacKintosh FC, Lubensky TC, Janmey P (2005) Nonlinear elasticity in biological gels. *Nature* 435:191–194.
2. Gardel M, et al. (2004) Elastic behavior of cross-linked and bundled actin networks. *Science* 304:1301–1305.
3. Stossel T, et al. (2001) Filamins as integrators of cell mechanics and signalling. *Nat Rev Mol Cell Biol* 2:138–145.
4. Nakamura F, et al. (2007) Structural basis of filamin A functions. *J Cell Biol* 179:1011–1025.
5. Gardel M, et al. (2006) Stress-dependent elasticity of composite actin networks as a model for cell behavior. *Phys Rev Lett* 96:088102.
6. Gardel M, et al. (2006) Prestressed F-actin networks cross-linked by hinged filamins replicate mechanical properties of cells. *Proc Natl Acad Sci USA* 103:1762–1767.
7. Wagner B, et al. (2006) Cytoskeletal polymer networks: The molecular structure of cross-linkers determines macroscopic properties. *Proc Natl Acad Sci USA* 103:13974–13978.
8. Kasza K, et al. (2009) Nonlinear elasticity of stiff biopolymers connected by flexible linkers. *Phys Rev E Stat Nonlin Soft Matter Phys* 79:041928.
9. Fernandez P, Pullarkat P, Ott A (2006) A master relation defines the nonlinear viscoelasticity of single fibroblasts. *Biophys J* 90:3796–3805.
10. Trepat X, et al. (2004) Viscoelasticity of human alveolar epithelial cells subjected to stretch. *Am J Physiol Lung Cell Mol Physiol* 287:L1025–L1034.
11. Pasternak C, Spudich J, Elson E (1999) Capping of surface receptors and concomitant cortical tension are generated by conventional myosin. *Nature* 341:549–551.
12. Wang N, et al. (2001) Mechanical behavior in living cells consistent with the tensegrity model. *Proc Natl Acad Sci USA* 98:7765–7770.
13. Wang N, et al. (2002) Cell prestress. I. Stiffness and prestress are closely associated in adherent contractile cells. *Am J Physiol* 282:C606–C616.
14. Stamenovic D, et al. (2004) Rheology of airway smooth muscle cells is associated with cytoskeletal contractile stress. *J Appl Physiol* 96:1600–1605.
15. Balland M, Richert A, Gallet F (2005) The dissipative contribution of myosin II in the cytoskeleton dynamics of myoblasts. *Eur Biophys J* 34:255–261.
16. Engler A, Sen S, Sweeney H, Discher D (2006) Matrix elasticity directs stem cell lineage specification. *Cell* 126:677–689.
17. Solon J, et al. (2007) Fibroblast adaptation and stiffness matching to soft elastic substrates. *Biophys J* 93:4453–4461.
18. Martens J, Radmacher M (2008) Softening of the actin cytoskeleton by inhibition of myosin II. *Pflugers Arch* 456:95–100.
19. Reichl E, et al. (2008) Interactions between myosin and actin crosslinkers control cytokinesis contractility dynamics and mechanics. *Curr Biol* 18:471–480.
20. Finer J, Simmons R, Spudich J (1994) Single myosin molecule mechanics: Piconewton forces and nanometre steps. *Nature* 368:113–119.
21. Stewart M, Kensler R (1986) Arrangement of myosin heads in relaxed thick filaments from frog skeletal muscle. *J Mol Biol* 192:831–851.
22. Verkhovsky A, Borisy G (1993) Non-sarcomeric mode of myosin II organization in the fibroblast lamellum. *J Cell Biol* 123:637–652.
23. Liverpool T, Maggs A, Ajdari A (2001) Viscoelasticity of solutions of motile polymers. *Phys Rev Lett* 86:4171–4174.
24. Humphrey D, et al. (2002) Active fluidization of polymer networks through molecular motors. *Nature* 416:413–416.
25. Ziebert F, Aranson I (2008) Rheological and structural properties of dilute active filament solutions. *Phys Rev E Stat Nonlin Soft Matter Phys* 77:011918.
26. Broedersz C, Storm C, MacKintosh F (2008) Nonlinear elasticity of composite networks of stiff biopolymers with flexible linkers. *Phys Rev Lett* 101:118103.
27. Furuike S, Ito T, Yamazaki M (2001) Mechanical unfolding of single filamin A (ABP-280) molecules detected by atomic force microscopy. *FEBS Lett* 498:72–75.
28. Straight A, et al. (2003) Dissecting temporal and spatial control of cytokinesis with a myosin II inhibitor. *Science* 299:1743–1747.
29. Mizuno D, Tardin C, Schmidt C, MacKintosh F (2007) Nonequilibrium mechanics of active cytoskeletal networks. *Science* 315:370–373.
30. Bendix P, et al. (2008) A quantitative analysis of contractility in active cytoskeletal protein networks. *Biophys J* 94:3126–3136.
31. Backouche F, Haviv L, Groswasser D, Bernheim-Groswasser A (2006) Active gels: Dynamics of patterning and self-organization. *Phys Biol* 3:264–273.
32. Semmrich C, Larsen R, Bausch A (2008) Nonlinear mechanics of entangled F-actin solutions. *Soft Matter* 4:1675–1680.
33. Brangwynne C, Koenderink G, Mackintosh F, Weitz D (2008) Nonequilibrium microtubule fluctuations in a model cytoskeleton. *Phys Rev Lett* 100:118104.
34. Gardel M, et al. (2004) Scaling of F-actin network rheology to probe single filament elasticity and dynamics. *Phys Rev Lett* 93:188102.
35. MacKintosh FC, Levine AJ (2008) Nonequilibrium mechanics and dynamics of motor-activated gels. *Phys Rev Lett* 100:018104.
36. Liverpool T, Marchetti M, Joanny J, Prost J (2009) Mechanical response of active gels. *Europhys Lett* 85:1800.
37. Tharmann R, Claessens MM, Bausch AR (2007) Viscoelasticity of isotropically cross-linked actin networks. *Phys Rev Lett* 98:088103.
38. Le Goff L, Amblard F, Furst E (2002) Motor-driven dynamics in actin-myosin networks. *Phys Rev Lett* 88:018101.
39. Janson E, Kolega J, Taylor D (1991) Modulation of contraction by gelation/solation in a reconstituted motile model. *J Cell Biol* 114:1005–1015.
40. MacKintosh F, Kas J, Janmey P (1995) Elasticity of semiflexible biopolymer networks. *Phys Rev Lett* 75:4425–4428.
41. Prassler J, et al. (1997) Interaction of a Dictyostelium member of the plastin/fimbrin family with actin filaments and actin-myosin complexes. *Mol Biol Cell* 8:83–95.
42. Lele T, et al. (2006) Mechanical forces alter zyxin unbinding kinetics within focal adhesions of living cells. *J Cell Physiol* 207:187–194.
43. Ferrer J, et al. (2008) Measuring molecular rupture forces between single actin filaments and actin-binding proteins. *Proc Natl Acad Sci USA* 105:9221–9226.
44. Voituriez R, Joanny J, Prost J (2006) Generic phase diagram of active polar films. *Phys Rev Lett* 96:028102.
45. Cates M, et al. (2008) Shearing active gels close to the isotropic-nematic transition. *Phys Rev Lett* 101:068102.
46. Ziebert F, Aranson I, Tsimring L (2007) Effects of cross-links on motor-mediated filament organization. *New J Phys* 9:421.
47. Matzke R, Jacobson K, Radmacher M (2001) Direct, high-resolution measurement of furrow stiffening during division of adherent cells. *Nat Cell Biol* 3:607–610.
48. Smith B, Tolloczko B, Martin J, Grutter P (2005) Probing the viscoelastic behavior of cultured airway smooth muscle cells with atomic force microscopy: Stiffening induced by contractile agonist. *Biophys J* 88:2994–3007.
49. Fabry B, et al. (2001) Scaling the microrheology of living cells. *Phys Rev Lett* 87:148102.
50. Deng L, et al. Fast and slow dynamics of the cytoskeleton (2006) *Nat Mater* 5:636–640.
51. Alcaraz J, et al. (2003) Microrheology of human lung epithelial cells measured by atomic force microscopy. *Biophys J* 84:2071–2079.
52. Cunningham C, et al. (1992) Actin-binding protein requirement for cortical stability and efficient locomotion. *Science* 255:325–327.
53. Hartwig J, Shevlin P (1986) The architecture of actin filaments and the ultrastructural location of actin-binding protein in the periphery of lung macrophages. *J Cell Biol* 103:1007–1020.
54. Kakugo A, Sugimoto S, Gong J, Osada Y (2002) Gel machines constructed from chemically cross-linked actin and myosins. *Adv Mater* 14:1124–1126.
55. Pardee J, Spudich J (1982) Purification of muscle actin. *Methods Enzymol* 85:164–181.
56. Kwiatkowski D, Janmey P, Yin H (1989) Identification of critical functional and regulatory domains in gelsolin. *J Cell Biol* 108:1717–1726.